



Bi-component Cu₂O–CuCl composites with tunable oxygen vacancies and enhanced photocatalytic properties

Renchun Yang*, Xiaojia Lu, Xiang Huang, Zhiming Chen, Xu Zhang,
Maodong Xu, Qingwu Song, Lingting Zhu

School of Biological and Chemical Engineering, Anhui Polytechnic University, Wuhu 241000, China



ARTICLE INFO

Article history:

Received 14 December 2014

Received in revised form 27 January 2015

Accepted 31 January 2015

Available online 2 February 2015

Keywords:

Bi-component

Cu₂O–CuCl composites

Oxygen vacancies

Photodecoloration

ABSTRACT

Bi-component Cu₂O–CuCl composites with tunable oxygen vacancies contents have been successfully fabricated via the introduction of Cl source using a simple hydrothermal reduction method. The morphology, composition and structure of the prepared catalysts were characterized by FE-SEM, HR-TEM, EDS, XRD, XPS, EPR, UV-vis DRS and N₂ adsorption–desorption. The O/Cl ratios of the microcube Cu₂O–CuCl composites can be easily tuned by the glucose amount. The results indicate that oxygen vacancies contents and E_g values of the as-prepared samples are heavily dependent on the O/Cl ratios. Compared with the single component Cu₂O sample, the Cu₂O–CuCl composites show higher oxygen vacancies contents and narrower band gaps. These findings reveal that the introduction of Cl promotes the efficiencies of light harvest and charge carrier separation, ultimately enhancing the photodecoloration performance of MB.

© 2015 Elsevier B.V. All rights reserved.

1. Introduction

Over the past decade, semiconductor photocatalysts have aroused great interest owing to their intriguing potential for resolving the current energy and environmental problems [1–3]. As an important family of metal oxides, cupric oxide (Cu₂O), is generally accepted as a promising photocatalyst due to its low cost, abundant and environment friendly characteristics [4–6]. Study indicates that the performance of these materials is closely related to their microstructures [7–9]. Thus, much effort has been devoted to design them via controlling the composition, crystallographic structure, and size, etc [10–12]. To date, although numerous Cu₂O nano/micro materials with different structures have been constructed, the wide spread use of Cu₂O material is limited due to the quick recombination of photo-generated charge carriers. Therefore, it is highly desired to develop strategies of suppressing the recombination of charge carriers.

Oxygen vacancies have been demonstrated to have crucial effects on the physical and chemical properties of semiconductor oxides [13–15]. More importantly, recent studies indicate that the presence of oxygen vacancies can effectively improve the photoabsorption and reduce the chance of charge recombination, ultimately resulting in an enhanced photocatalytic performance [16,17]. Thus,

much effort has been devoted to construct the oxygen vacancies. For generating oxygen vacancies, one of the popular strategies is the heat treatment in a reducing atmosphere [18–20]. However, most of these methods often need relatively complicated equipments and rigorous conditions, such as high temperature and high pressure. Another prevalent approach to produce oxygen vacancies is the replacement of lattice oxygen via introducing a foreign species, such as doping or forming heterostructure [21–23]. Among various foreign species, nonmetal elements, especially for N [24], C [25] and S [26], have been confirmed holding specific promoting effect for forming oxygen vacancies and to enhance catalytic performance [27]. Clearly, oxygen vacancies can be modulated with a relatively simple route and mild conditions in this way. Besides N, C and S, recent studies indicate that halogen is also one type of promoting agent for generating oxygen vacancies [28–33]. However, compared to the gained progress on halogen modified TiO₂ [31–33], there are relatively limited reports on the modification of other semiconductor with halogens [28–30], especially for Cl modified Cu₂O. Therefore, it should be interesting to construct Cl modified Cu₂O composites and to explore its application as photocatalyst.

Motived by the above mentioned advantages, an economical and facile method, hydrothermal reduction, is introduced to fabricate oxygen vacancies in this work. Here, we prepared cubic Cu₂O–CuCl composites via D-(+)-glucose reducing CuCO₃·Cu(OH)₂ and using NaCl as Cl source. By controlling the amount of glucose, cubic Cu₂O–CuCl composites with tunable oxygen vacancies contents and Cu₂O/CuCl component ratios were suc-

* Corresponding author. Tel.: +86 553 2871255.

E-mail address: yrclq@163.com (R. Yang).

cessfully fabricated. The process is facile, low-cost and green since only water, sodium chloride, copper carbonate basic and D-glucose were introduced. Moreover, the contrastive studies of structure and photocatalytic performance of the Cu₂O–CuCl composites and single component Cu₂O were investigated in detail.

2. Experimental

2.1. Synthesis of Cu₂O–CuCl

In a typical synthesis of Cu₂O–CuCl composites, 240 mg of CuCO₃·Cu(OH)₂ powder was first added to a 50 mL Teflon-lined stainless steel autoclave. Subsequently, 64 mg sodium chloride, 40 mg of D-(+)-glucose powder and 10 mL deionized water were added with stirring. The autoclave was sealed and heated at 200 °C for 24 h, then allowed to cool down to room temperature naturally. When the reaction was finished, the obtained product was collected by centrifugation, and washed with deionized water three times. Then the sample was dried at ambient temperature under vacuum for 12 h. The resultant sample was designated Cu₂O–CuCl40 (40 representing the amount glucose). To study the effects of the amount of D-glucose on the structure of the Cu₂O–CuCl composite, the other two samples were also prepared with the amount of D-glucose at 37 mg and 43 mg and keeping other conditions unchanged, which are named as Cu₂O–CuCl37 and Cu₂O–CuCl43, respectively. In addition, to obtain contrastive study of structure and photocatalytic performance, the Cu₂O sample was also prepared using similar conditions as those of the Cu₂O–CuCl40. The only difference between them is that sodium chloride was not introduced in the preparation process of the Cu₂O.

2.2. Structural characterizations

The morphologies and structures of the samples were characterized using a scanning electron microscope (FE-SEM, Hitachi S4800) and a transmission electron microscope (TEM, JEM-2010). The element mapping distribution of the samples was acquired by a Horiba EX-250 energy dispersive X-ray spectrometry (EDS) operated at 20.0 kV, associated with FE-SEM. Powder X-ray Diffraction patterns of the samples were obtained with a Rigaku diffractometer/MAX-RB by nickel-filtered Cu K α radiation ($\lambda = 154.18 \text{ pm}$). Diffraction patterns were recorded over a range of 2 θ angles from 20° to 80° using a 0.02° step size. Thermo ESCALAB 250 XPS Spectrometer, with Al K α radiation, was used for obtaining XPS data. In XPS study, C 1s-binding energy value of 285 eV was taken as a reference level. The electron paramagnetic resonance (EPR) spectra measurement was carried out using an Endorspectrometer (JEOL ES-ED3X) at room temperature. The g factor was obtained by taking the signal of manganese as standard. Ultraviolet-visible diffuse reflectance spectroscopy (UV-vis DRS, Hitachi U-3900) was performed in the range of 200–800 nm with integrating sphere attachment and spectral on reflectance standards. The porosity characteristics of the catalysts were determined by nitrogen adsorption–desorption (NOVA 2000e).

2.3. Catalytic testing

The evaluation of photocatalytic activity of the as-prepared samples for the photocatalytic decolorization of methylene blue (MB) solution was performed on photocatalytic reactor (BL-GHX, Shanghai Bilang Instrument Co., Ltd.) at 20 °C. The vis light intensity of about 0.2 W cm⁻² was obtained by a Xe lamp with glass filters. In a typical process, 50 mg of the prepared powders were dispersed in a quartz vessel containing 100 mL of 10 mg L⁻¹ MB aqueous solution. Before illumination, the mixture in the quartz

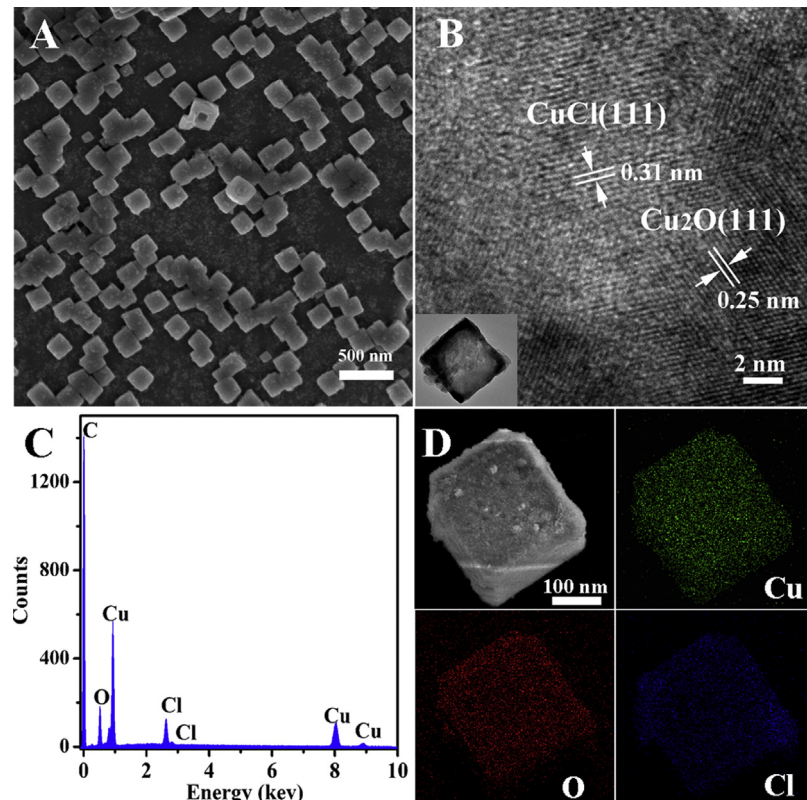


Fig. 1. SEM image (A), TEM image (B), EDS spectrum (C), and EDS mapping (D) of the sample Cu₂O–CuCl40 composite.

vessel was constantly stirred for 1 h in dark to ensure the establishment of an adsorption–desorption equilibrium between the photocatalyst and MB. After that, the quartz vessel was irradiated with light from a 500 W xenon lamp with cutoff filter (providing visible light with a wavelength longer than 400 nm). At each given time interval, 5 mL of the mixture solution was taken out every 1 h during irradiation. After centrifugation, the solution was detected by UV-vis absorption spectra.

3. Results and discussion

3.1. Analysis of the microcube Cu₂O–CuCl

The morphology and composition of the Cu₂O–CuCl40 sample were characterized by SEM, TEM and EDS; results are shown in Fig. 1. As can be seen in Fig. 1A, SEM image shows that the products consisted of uniform cubic shape microcrystals. The length of the side of the microcube is about 200 nm. Further information observation about the Cu₂O–CuCl40 sample was obtained from the HR-TEM image (Fig. 1B). From the HR-TEM image, it can be seen that interlayer distances of the selected area are calculated to be 0.31 nm and 0.25 nm, which are ascribed to the (1 1 1) and (1 1 1) crystal planes of CuCl and Cu₂O, respectively. Such result demonstrates that Cu₂O and CuCl may coexist in the cubic shape microcrystals. In addition, from the TEM image (insert image), one can easily find that the strong color contrast exists among the whole microcrystal area, indicating that the cubic shape microcrystal is not a solid structure. The EDS element analysis (Fig. 1C) shows that the sample includes four elements (Cu, O, Cl, and C). Among them, the signal of C should be ascribed to the anisotropic conductive film, while the signals of Cu, O, and Cl are attributed to the Cu₂O–CuCl40 sample, revealing that the sample may be consisted of two components (Cu₂O and CuCl). As displayed in Fig. 1D, elemental mapping analysis provides tangible evidence that Cu, O,

and Cl atoms are homogeneously distributed throughout the whole composite microcrystal.

3.2. Morphology characterization

To study the effect of glucose on the product, a series of experiments have been performed by only changing the amount of glucose and keeping other conditions unchanged. As can be seen in Fig. 2a–c, the amount of glucose plays a very important role on controlling the morphologies of Cu₂O–CuCl composites. The most distinct phenomenon is that the sizes of the Cu₂O–CuCl microcrystals can be adjusted by the amount of glucose. When the adding amount of glucose is 37 mg, relative big Cu₂O–CuCl microcubes with a side length of about 350 nm can be found in the product (Fig. 2a). With the increase of glucose amount to 40 mg, relative small Cu₂O–CuCl microcrystals with the size about 200 nm have been obtained (Fig. 2b). Further increase of the amount of glucose to 43 mg resulted in smaller Cu₂O–CuCl microcrystals with the size about 100 nm (Fig. 2c). As we known, the crystal growth rate would increase with the rise of concentration of reactant [34]. Thus, the size evolution with the glucose concentration could be due to the controlled kinetics effect [35]. As a result, the higher the amount of glucose was offered, the smaller the size of the microcubes presented. The other marked phenomenon is that the effect of Cl[−] ions on the morphology of the product. Obviously, without Cl[−] ions, only irregular particles with relatively small size about 80 nm presented (Fig. 2d), whereas the obtained products all evolved to uniform microcubes when Cl[−] ions were introduced (Fig. 2a–c). Such result should be ascribed to nature characteristics. It is well known that the copper oxides belongs cubic crystal system and cubic Cu₂O nano/microparticles are easily obtained. Thus, the Cu₂O–CuCl composites should be attributed to the cubic crystal system. However, no cubic structure Cu₂O can be found. Such result should be ascribed to the unfinished Ostwald ripening process of

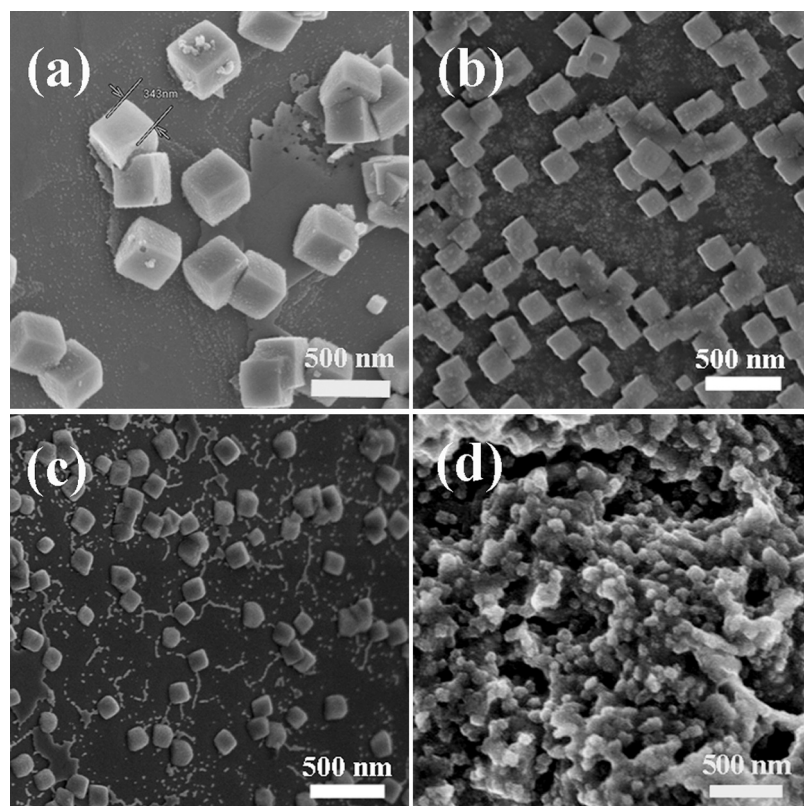


Fig. 2. SEM images of the samples: (a) Cu₂O–CuCl37, (b) Cu₂O–CuCl40, (c) Cu₂O–CuCl43 and (d) Cu₂O.

Table 1

Surface areas, grain sizes and compositions of various samples.

Sample	Surface area ($\text{m}^2 \text{ g}^{-1}$)	Average size ^a (nm)		Atomic ratio ^b	
		Cu ₂ O	CuCl	Cl/O	O _{ads} /O _{latt}
Cu ₂ O–CuCl37	11.8	45.3	37.6	0.40	2.5
Cu ₂ O–CuCl40	12.3	35.5	27.3	0.47	3.7
Cu ₂ O–CuCl43	12.6	28.3	21.7	0.56	4.9
Cu ₂ O	12.1	32.6	—	—	2.3

^a These data obtained by the Scherrer's equation analysis.

^b Data based on quantitative analysis of XPS.

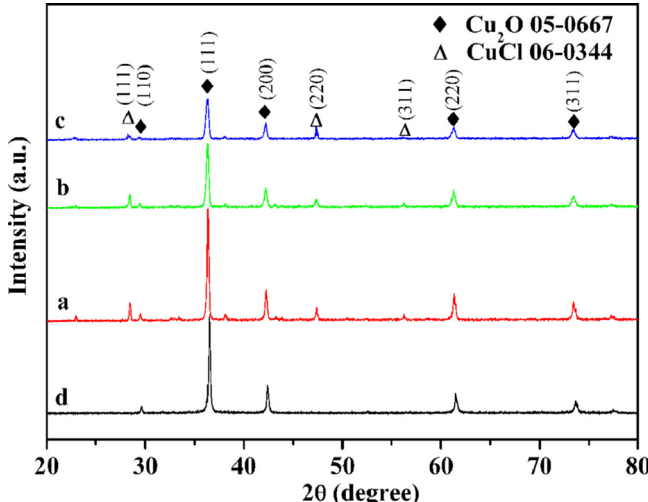


Fig. 3. XRD patterns of the samples: (a) Cu₂O–CuCl37, (b) Cu₂O–CuCl40, (c) Cu₂O–CuCl43 and (d) Cu₂O.

Cu₂O since their sizes are all smaller than those of the Cu₂O–CuCl microcrystals.

XRD measurements were conducted to investigate the composition of the resultant samples as shown in Fig. 3. As for the Cu₂O sample (Fig. 3d), all the sharp diffraction peaks can be readily assigned to the cubic phase of cuprite (JCPDS 05-0067). Apparently, no other substances were discovered. However, for the samples prepared via introducing Cl (Fig. 3a–c), two types of crystal phases peaks appeared simultaneously. A matching with JADE indicates that the diffraction peaks at 28.5°, 47.4° and 56.3° are assigned to the (1 1 1), (2 2 0) and (3 1 1) planes of crystal phases CuCl (JCPDS 06-0344), while the peaks at 36.4°, 42.4° and 61.3° are attributed to the (1 1 1), (2 0 0) and (2 2 0) crystal planes of Cu₂O (JCPDS 05-0067). Such result clearly indicates that the two components (Cu₂O and CuCl) coexist in the samples, confirming the foregoing HR-TEM and EDS analysis that the resultant products are bi-component Cu₂O–CuCl composite. Furthermore, to study the sizes of two components, the two strongest peaks of Cu₂O (36.4°) and CuCl (28.5°) were calculated based on Scherrer's equation and the results are shown in Table 1. As can be seen, for the Cu₂O–CuCl37 sample, the average crystallite sizes of Cu₂O and CuCl are about 45.3 nm and 37.6 nm, respectively, indicating that the obtained Cu₂O–CuCl microcubes are composed of some smaller nano-particles. With the increase of the amount of glucose, the crystallite sizes of Cu₂O and CuCl all decreased rapidly. Such result suggests that not only the sizes of Cu₂O–CuCl microcubes but also the sizes of Cu₂O and CuCl particles all could be reduced with the increase of glucose amount.

3.4. XPS analysis

More detailed information on the chemical composition, surface electronic state and oxygen vacancy of the samples were acquired from XPS and the result are shown in Fig. 4. The

spectra a, b, c and d profiles represent the samples Cu₂O–CuCl37, Cu₂O–CuCl40, Cu₂O–CuCl43 and Cu₂O, respectively. Peak areas of the recorded spectra were estimated by fitting the curves with combination of Gaussian curves of variable proportion [36]. The surface element compositions of O/Cl and O_{ads}/O_{latt} ratios are given in Table 1. Fig. 4A shows a typical XPS survey spectrum of the sample Cu₂O–CuCl40. It can be clearly observed that Cu, O, Cl and C four elements exist in the spectrum, among which the signal of C should be ascribed to the absorbed carbon dioxide.

High-resolution XPS spectra for Cu 2p, O 1s and Cl 2p regions are used to deeply evaluate the binding behavior of the elements in various samples; results are shown in Fig. 4B–D. As shown in Fig. 4B, a typical Cu 2p XPS spectrum of the samples exhibit two predominant characteristic peaks around 932.0–932.5 and 951.5–952.4 eV, which are attributed to Cu 2p_{3/2} and Cu 2p_{1/2} of Cu₂O, respectively [37]. Through observation, one can easily find that the peak positions of the Cu₂O–CuCl samples are not consistent with those of the Cu₂O sample. Distinctly, compared with the Cu₂O sample, the Cu₂O–CuCl samples show a relative low binding energy value for Cu 2p XPS spectra. It is generally acknowledged that the bonding energy of a component is usually affected by its surrounding chemical environment [38]. With the introduction of Cl, the bonding energy negative shift occurs for the peak of Cu 2p, implying that Cu in Cu₂O–CuCl sample gains electrons from Cl and thus becomes electron-rich. Moreover, with the increase of glucose, the negative shift of the Cu 2p bonding energy present more markedly as shown in the samples Cu₂O–CuCl37, Cu₂O–CuCl40 and Cu₂O–CuCl43 (Table 1), suggesting that the introduction of Cl play an important role on surface electronic state.

Fig. 4C shows the O 1s region of the X-ray photoelectron spectra. The spectra of the four samples all show two peaks around at 530.5 and 531.8 eV. The characteristic line at 530.5 eV was attributed to surface lattice oxygen (O_{latt}) species, whereas the peak located at 531.8 eV was ascribed to the adsorbed oxygen (O_{ads}) species [39,40]. By quantitatively analyzing the spectra, one can easily observe that there was a distinct difference in O_{ads}/O_{latt} molar ratio of the four samples. As shown in Table 1, the O_{ads}/O_{latt} molar ratios of the three Cu₂O–CuCl samples are markedly higher than that of the Cu₂O sample, suggesting that the introduction of Cl results in O_{ads}-enriched on the surface of the samples. More evidently, with the increase of Cl content, O_{ads}/O_{latt} molar ratios also increase. Obviously, the Cu₂O–CuCl43 sample exhibits the highest O_{ads}/O_{latt} molar ratio (4.3), indicating that higher Cl content is beneficial for the enhancement of O_{ads} oxygen species. It is generally accepted that O_{ads} oxygen species are mainly affected by surface oxygen vacancies [41,42] since they are often adsorbed only by the oxygen vacancies at vacuum conditions. Thus, more oxygen vacancies should occur on the sample with higher O_{ads} species content, which are responsible for the higher activity of photocatalysis [18].

Fig. 4D exhibits the Cl 2p region of the X-ray photoelectron spectra. As can be seen, the Cl 2p peak shows two components at 198.4 eV and 200.1 eV, which are assigned to Cl 2p_{3/2} and Cl 2p_{1/2} of CuCl, respectively [43,44]. It can be found that the most distinct difference among the three Cu₂O–CuCl samples is the peak

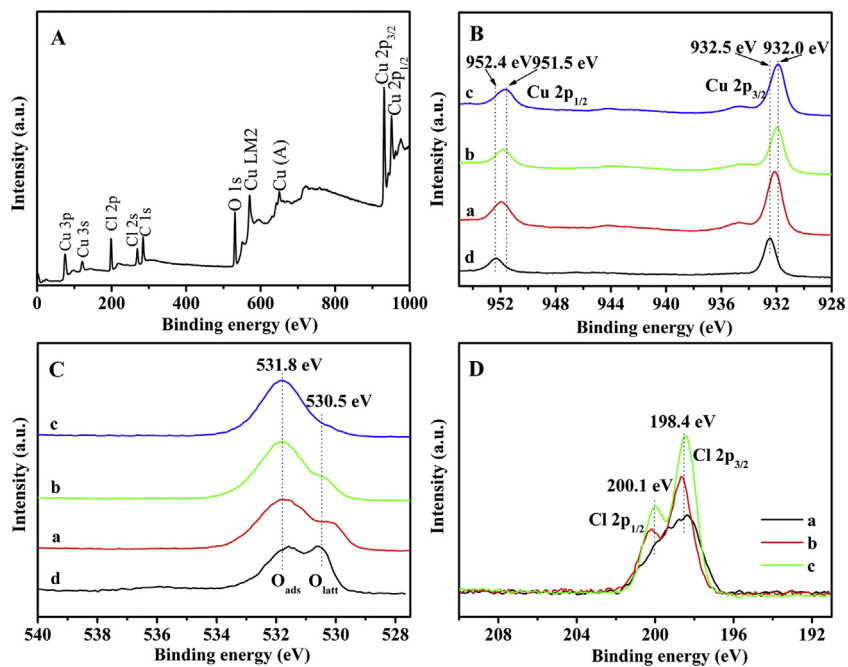


Fig. 4. XPS spectra of the Cu_2O – CuCl and Cu_2O samples: (A) full survey spectrum, (B) Cu 2p, (C) O 1s and (D) Cl 2p; curves a, b, c, d corresponding to Cu_2O – CuCl37 , Cu_2O – CuCl40 , Cu_2O – CuCl43 and Cu_2O , respectively.

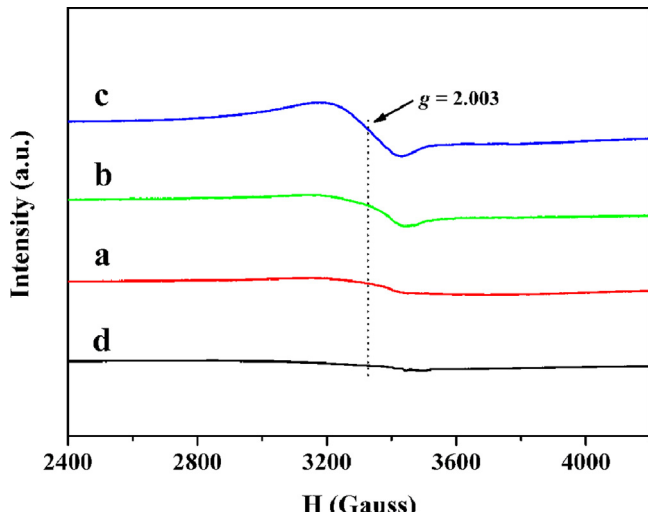


Fig. 5. Room-temperature EPR spectra of the samples: (a) Cu_2O – CuCl37 , (b) Cu_2O – CuCl40 , (c) Cu_2O – CuCl43 and (d) Cu_2O .

intensity. Generally, the peak intensity of a composition represents its content. Thus, the Cl content of the three samples follows the order: Cu_2O – $\text{CuCl37} < \text{Cu}_2\text{O}$ – $\text{CuCl40} < \text{Cu}_2\text{O}$ – CuCl43 , which is also conformed by Cl/O molar ratios (as shown in Table 1). From the analysis of Fig. 4B–D, one can find that the rise of the addition amount of glucose not only promoted the negative shift of the Cu 2p bonding energy but also resulted in an enhanced oxygen vacancies content.

3.5. EPR analysis

It is generally acknowledged that EPR can provide sensitive and direct information on monitoring various behaviors of native defects, such as oxygen vacancies. To study the effects of the chemical compositions on the oxygen defects, the samples were characterized by EPR; results are shown in Fig. 5. Obviously, the

Cu_2O sample is EPR silent, suggesting that no localized unpaired electrons present in the single component Cu_2O sample. However, when Cl element was introduced into the samples, the three Cu_2O – CuCl samples all displayed resonance signal at $g=2.003$, which should be attributed to the presence of oxygen vacancies. Such result indicates that the introduction of Cl promoted the formation of oxygen vacancies. Similar results were also confirmed that the presence of halogen (F^- ions) can create oxygen vacancies [27,45]. More remarkably, with the increase of Cl content, the peak intensities of EPR signal also increased. Clearly, the Cu_2O – CuCl43 sample exhibits the highest EPR signal, suggesting that a higher Cl content is helpful to enhancing the oxygen vacancies content, in agreement with the foregoing XPS analysis. It is generally accepted that the oxygen vacancies often play a crucial role in surface applications such as heterogeneous catalysis. Recent studies indicate that higher photocatalysis activity can be achieved by the oxygen vacancies owing to the formation of narrow band gap [46,47]. Thus, the Cu_2O – CuCl samples cloud present higher catalytic active than that of the Cu_2O sample, although their have similar specific surface areas (Table 1).

3.6. UV-vis DRS analysis

To ascertain the optical property of the as-prepared samples, the optical experiment was investigated by UV-vis DRS spectroscopy. As shown in Fig. 6A, the three Cu_2O – CuCl samples all exhibit a broad absorption band from 200 to 800 nm. Distinctly, the optical absorptions of the Cu_2O – CuCl samples are stronger than that of the Cu_2O sample at the visible light region. Such phenomenon should be assigned to the existence of oxygen vacancies [16,17], indicating that the Cu_2O – CuCl samples are more effective visible light response material. However, the increase for the optical absorption intensity is not always going on with the rise of the Cl/O molar ratio, suggesting that the optimum synergistic effect between Cu_2O and CuCl should exist for the optical absorption.

The equation $(\alpha h\nu)^2 = K(h\nu - E_g)$ was used to calculate the band gap of the samples, where α is the absorption coefficient, K is a proportionality constant, and E_g is the band-gap energy [48]. As

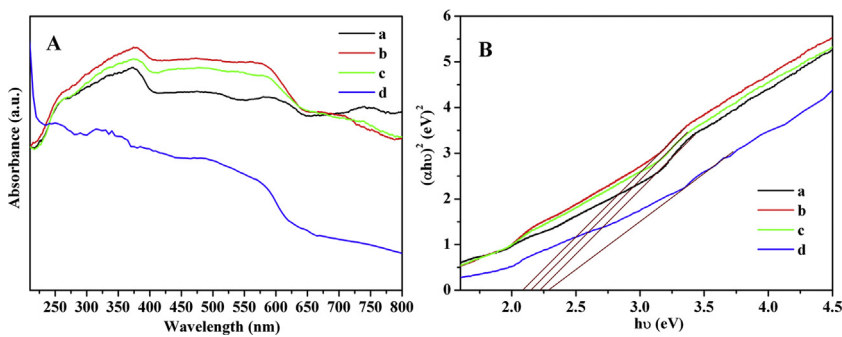


Fig. 6. (A) UV-vis absorption spectrums and (B) the corresponding plots of $(\alpha h\nu)^2$ vs. $h\nu$ curves for the samples: (a) $\text{Cu}_2\text{O}-\text{CuCl37}$, (b) $\text{Cu}_2\text{O}-\text{CuCl40}$, (c) $\text{Cu}_2\text{O}-\text{CuCl43}$ and (d) Cu_2O .

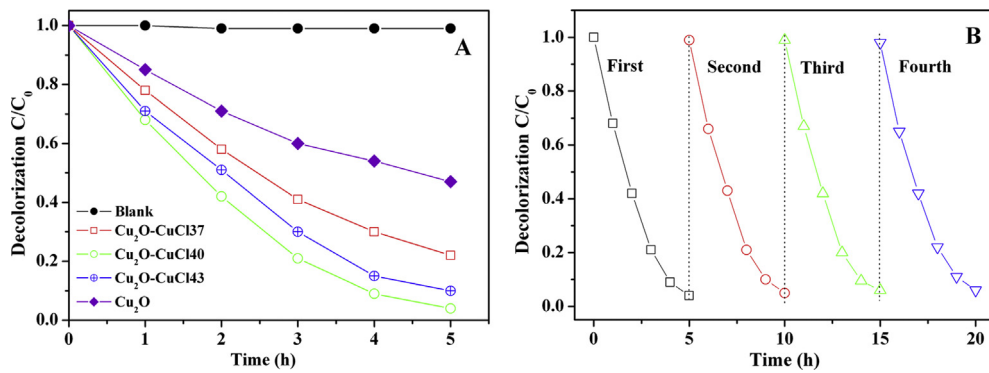


Fig. 7. (A) The photocatalysis activities of the catalysts; (B) cyclic photocatalysis decolorization performance for the $\text{Cu}_2\text{O}-\text{CuCl40}$ sample.

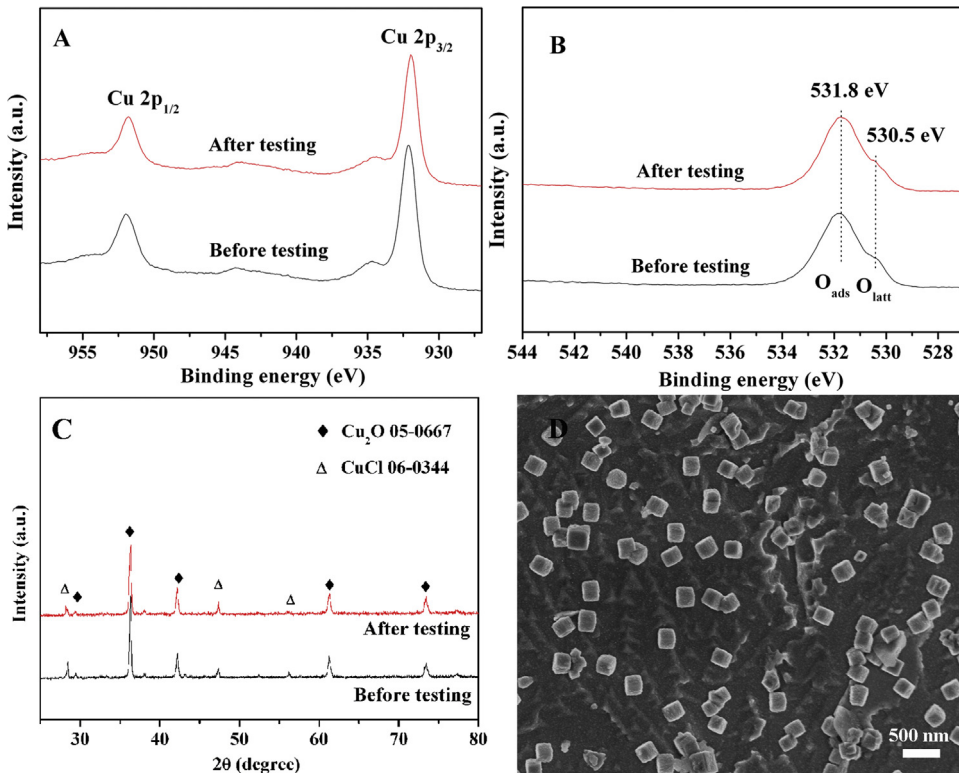


Fig. 8. (A, B) Cu 2p and O 1s XPS and (C) XRD of the $\text{Cu}_2\text{O}-\text{CuCl40}$ sample before and after testing; (D) SEM of the $\text{Cu}_2\text{O}-\text{CuCl40}$ sample after testing.

can be seen in Fig. 6B, the optical band gaps (E_g) are estimated to be about 2.22, 2.12, 2.16 and 2.30 for the Cu₂O–CuCl37, Cu₂O–CuCl40, Cu₂O–CuCl43 and Cu₂O samples, respectively. Obviously, the optical band gaps (E_g) of the Cu₂O–CuCl samples are less than that of the single Cu₂O sample, indicating that the band gap stronger depends on the chemical composition. The decrease of band gap for the Cu₂O–CuCl samples indicates that light harvest and charge carrier separation can be achieved more easily, which should be helpful to improve photocatalytic reaction efficiencies [49]. Similar results have been demonstrated in previous photocatalysts [50]. However, the increase of the Cl/O molar ratio is not always helpful to decreasing the band gap. As can be seen, the band gap increases first and then decreases as the increase of Cl/O molar ratio, which is similar as the change trend of their optical absorption, revealing that the Cl/O molar ratio is a very prominent influence factor for the optical effect of the Cu₂O–CuCl composite.

3.7. Photocatalytic activity and reaction mechanism analysis

To evaluate the as-synthesized samples, the decoloration of MB under visible light irradiation as a function of the time was used to monitor the catalytic properties. As can be seen in Fig. 7A, after visible light irradiation for 5 h, the photocatalysis decolorization ratios of the blank sample, Cu₂O–CuCl37, Cu₂O–CuCl40, Cu₂O–CuCl43 and Cu₂O are about 0, 78, 96, 90 and 53%, respectively. Obviously, the catalytic properties of the Cu₂O–CuCl samples are all superior to that of the single Cu₂O sample. The repeatability of photodegradation performance for MB was also investigated. As shown in Fig. 7B, no obvious decrease of decoloration was observed after the four cycles under 20 h visible light irradiation. Moreover, to study the stability, SEM, XRD and XPS characterizations of the optimal Cu₂O–CuCl40 sample after four cycles testing were also performed. As can be seen in Fig. 8, no distinct difference can be found in this case, suggesting that the as-prepared sample is a stable photocatalyst in the reactions.

According to foregoing analysis, one can easily find that the main differences between the Cu₂O–CuCl samples and the Cu₂O sample are their chemical constitutions, especially for their oxygen vacancies contents. Obviously, the presence of higher catalytic performance for the Cu₂O–CuCl samples than that of the Cu₂O sample should be ascribed to the oxygen vacancies content and the E_g band gap. Based on foregoing XPS, EPR and UV-vis spectroscopy, one can find that the Cu₂O–CuCl samples exhibit higher oxygen vacancies contents and lower E_g values than those of the Cu₂O sample. Clearly, the introduction of Cl influences the Cl/O ratio, which promotes the formation of oxygen defects of the samples, ultimately resulting in a decreased E_g value. Thus, a potential process may occur that the value band width can be narrowed due to the formation of oxygen vacancies. As we know, the high oxygen vacancies content and the low optical band gap are beneficial to improving the photoabsorption and reduce the chance of charge recombination. As a result, the Cu₂O–CuCl samples possessing more oxygen vacancies showed higher catalytic activities than that of the Cu₂O sample.

4. Conclusions

In summary, bi-component Cu₂O–CuCl composites have been successfully fabricated via a simple hydrothermal reduction method. The O/Cl ratios of the microcube Cu₂O–CuCl composites can be easily tuned by the glucose amount. The results indicate that the two important influence factors (oxygen vacancies content and E_g band gap) for the photocatalyst are heavily dependent on the O/Cl ratios of the as-prepared samples. Compared with the single Cu₂O sample, the Cu₂O–CuCl composites showed better photodecoloration of MB under visible light, which might be

attributed to the more oxygen vacancies and lower E_g value. This research provides a promising route to prepare the Cu₂O–CuCl composite as photocatalyst with high catalytic activity.

Acknowledgments

This work is supported by National Nature Science Foundation of China (51202003 and 21471002), Natural Science Foundation of the Higher Education Institutions of Anhui Province, China (KJ2012A036) and National College Student Innovation Imbark Training Program Foundation of China (201310363064 and 201410363072).

References

- M. Setvín¹, U. Aschauer, P. Scheiber, Y. Li, W. Hou, M. Schmid, A. Selloni, U. Diebold¹, *Science* 341 (2013) 988–991.
- W. Wang, X. Huang, S. Wu, Y. Zhou, L. Wang, H. Shi, Y. Liang, B. Zou, *Appl. Catal. B: Environ.* 134 (2013) 293–301.
- M.A. Shoeib, O.E. Abdelsalam, M.G. Khafagi, R.E. Hammam, *Adv. Powder Technol.* 23 (2012) 298–304.
- A.T. Marin, D. Muñoz-Rojas, D.C. Iza, T. Gershon, K.P. Musselman, J.L. MacManus-Driscoll¹, *Adv. Funct. Mater.* 23 (2013) 3413–3419.
- N. Helalí, Y. Bessekhouad, A. Bouguelia, M. Trari, *Sol. Energy* 84 (2010) 1187–1192.
- B. Shaabani, E. Alizadeh-Gheshlaghi, Y. Azizian-Kalandaragh, A. Khodayari, *Adv. Powder Technol.* 25 (2014) 1043–1052.
- A. Hecia, A.W. Morawski, B. Grzmil, S. Mozia, *Appl. Catal. B: Environ.* 140 (2013) 108–114.
- M. Sankar, N. Dimitratos, P.J. Miedziak, P.P. Wells, C.J. Kiely, G.J. Hutchings, *Chem. Soc. Rev.* 41 (2012) 8099–8139.
- D. Liu, Y. Fernández, O. Ola, S. Mackintosh, M. Maroto-Valer, C.M.A. Parlett, A.F. Lee, J.C.S. Wu, *Catal. Commun.* 25 (2012) 78–82.
- J.F. de Brito, A.R. Araujo, K. Rajeshwar, M.V.B. Zanoni, *Chem. Eng. J.* 264 (2015) 302–309.
- Q. Hua, T. Cao, X. Gu, J. Lu, Z. Jiang, X. Pan, L. Luo, W. Li, W. Huang, *Angew. Chem. Int. Ed.* 126 (2014) 4956–4961.
- X. Guo, W. Lv, X. Li, *J. Phys. Chem. C* 118 (2014) 11062–11077.
- T.T. Chen, I.C. Chang, M.H. Yang, H.T. Chiu, C.Y. Lee, *Appl. Catal. B: Environ.* 142–143 (2013) 442–449.
- K. Yi Lee, Y.J. Huang, *Appl. Catal. B: Environ.* 150–151 (2014) 506–514.
- Q. Wu, R. van de Krol, *J. Am. Chem. Soc.* 134 (2012) 9369–9375.
- Z.H. Wei, J.M. Sun, Y. Li, A.K. Datye, Y. Wang, *Chem. Soc. Rev.* 41 (2012) 7994–8008.
- M. Li, Y. Hu, S. Xie, Y. Huang, Y. Tong, X. Lu, *Chem. Commun.* 50 (2014) 4341–4343.
- X. Chen, L. Liu, P.Y. Yu, S.S. Mao, *Science* 331 (2011) 746–750.
- F. Cheng, T. Zhang, Y. Zhang, J. Du, X. Han, J. Chen, *Angew. Chem. Int. Ed.* 52 (2013) 2474–2477.
- M. Samiee, L. Luo, *Mater. Lett.* 98 (2013) 205–208.
- H. Lia, S. Yin, Y. Wang, T. Sekino, S.W. Lee, T. Sato, *J. Catal.* 297 (2013) 65–69.
- G. Yang, T. Wang, B. Yang, Z. Yan, S. Ding, T. Xiao, *Appl. Surf. Sci.* 287 (2013) 135–142.
- J.A. Schiemer, R.L. Withers, Y. Liu, M.A. Carpenter, *Chem. Mater.* 25 (2013) 4436–4446.
- Y. Wang, C. Feng, M. Zhang, J. Yang, Z. Zhang, *Appl. Catal. B: Environ.* 100 (2010) 84–90.
- F. Dong, S. Guo, H. Wang, X. Li, Z. Wu, *J. Phys. Chem. C* 115 (2011) 13285–13292.
- S.H. Nam, T.K. Kim, J.H. Boo, *Catal. Today* 185 (2012) 259–262.
- A.E. Giannakas, E. Seristatidou, Y. Deligiannakis, I. Konstantinou, *Appl. Catal. B: Environ.* 132–133 (2013) 460–468.
- V. Kumar, A. Govind, R. Nagarajan, *Inor. Chem.* 50 (2011) 5637–5645.
- G. Huang, Y. Zhu, *Cryst. Eng. Comm.* 14 (2012) 8076–8082.
- F. Biccari, C. Malerba, A. Mittiga, *Sol. Energ. Mat. Sol. C* 94 (2010) 1947–1952.
- T.R. Gordon, M. Cargnello, T. Paik, F. Mangolini, R.T. Weber, P. Fornasiero, C.B. Murray, *J. Am. Chem. Soc.* 134 (2012) 6751–6761.
- R. Yuan, T. Chen, E. Fei, J. Lin, Z. Ding, J. Long, Z. Zhang, X. Fu, P.L. Wu, X. Wang, *ACS Catal.* 1 (2011) 200–206.
- L. Zhang, J. Zhou, J. Li, G. Liu, X. Lin, B. Mao, R. Liu, S. Zhang, J. Wang, *J. Phys. Chem. C* 118 (2014) 13726–13732.
- B. Heng, T. Xiao, W. Tao, X. Hu, X. Chen, B. Wang, D. Sun, Y. Tang, *Cryst. Growth Des.* 12 (2012) 3998–4005.
- H. Zhang, M. Jin, Y. Xia, *Angew. Chem. Int. Ed.* 51 (2012) 7656–7673.
- J.H. Scofield, *J. Electr. Spectrosc. Relat. Phenom.* 8 (1976) 129–137.
- Q. Hua, T. Cao, X. Gu, J. Lu, Z. Jiang, X. Pan, L. Luo, W. Li, W. Huang, *Angew. Chem. Int. Ed.* 126 (2014) 4956–4961.
- F. Mariño, G. Baronetti, M. Jobbagy, M. Laborde, *Appl. Catal. A: Gen.* 238 (2003) 41–54.
- A. Machocki, T. Ioannides, B. Stasinska, W. Gac, G. Avgouropoulos, D. Delimaris, W. Grzegorczyk, S. Pasieczna, *J. Catal.* 227 (2004) 282–296.

- [40] Y. Liu, H. Dai, Y. Du, J. Deng, L. Zhang, Z. Zhao, C. Au, *J. Catal.* 287 (2012) 149–160.
- [41] B.P. Barbero, J.A. Gamboa, L.E. Cadús, *Appl. Catal. B: Environ.* 65 (2006) 21–30.
- [42] Y. Zhu, Y. Sun, X. Niu, F. Yuan, H. Fu, *Catal. Lett.* 135 (2010) 152–158.
- [43] H. Altass, A.F. Carley, P.R. Davies, R.J. Davies, *Chem. Commun.* 49 (2013) 8223–8225.
- [44] J. Qiu, Y. Zhang, Y. Shen, Y. Zhang, H. Zhang, J. Liu, *Appl. Surf. Sci.* 256 (2010) 3274–3280.
- [45] C.D. Valentini, E. Finazzi, G. Pacchioni, A. Selloni, S. Livraghi, M.C. Paganini, E. Giannello, *Chem. Phys.* 339 (2007) 44–56.
- [46] Y. Lv, C. Pan, X. Ma, R. Zong, X. Bai, Y. Zhu, *Appl. Catal. B: Environ.* 138–139 (2013) 26–32.
- [47] L. Zhang, L. Wang, Y. Zhu, *Adv. Func. Mat.* 17 (2007) 3781–3790.
- [48] Z. Jiao, Y. Zhang, H. Yu, G. Lu, J. Ye, Y. Bi, *Chem. Commun.* 49 (2012) 636–638.
- [49] S. Xu, J. Ng, X. Zhang, H. Bai, D. Sun, *Int. J. Hydrogen Energ.* 35 (2010) 5254–6568.
- [50] Y. Shang, D. Sun, Y. Shao, D. Zhang, L. Guo, S. Yang, *Chem. Eur. J.* 18 (2012) 14261–14266.